Linkage of Posterior Amorphous Corneal Dystrophy to Chromosome 12q21.33 and Exclusion of Coding Region Mutations in *KERA*, *LUM*, *DCN*, and *EPYC*

Anthony J. Aldave,[1] *George O. D. Rosenwasser,*[2] *Vivek S. Yellore,*[1] *Jeanette C. Papp,*[3] *Eric M. Sobel,*[3] *Michele N. Pham,*[1] *Michael C. Chen,*[1] *Sugandha Dandekar,*[3] *Ram Sripracha,*[3] *Sylvia A. Rayner,*[1] *Joseph W. Sassani,*[4] *and Michael B. Gorin*[1]

Purpose. To identify the genetic basis of posterior amorphous corneal dystrophy (PACD) segregating in a large pedigree.

Methods. The authors performed clinical evaluation of a previously unreported pedigree with PACD, light and electron microscopic examination of an excised corneal button, genomewide linkage analysis, fine mapping linkage and haplotype analysis, and screening of four candidate genes (*KERA*, *LUM*, *DCN*, and *EPYC*).

Results. Twenty-one participants were determined to be affected based on the presence of characteristic clinical features of PACD; 15 affected and 39 unaffected individuals from a single pedigree enrolled in the study and provided DNA for analysis. Histopathologic examination of an excised corneal specimen from an affected individual demonstrated disorganized stromal lamellae and stromal staining with colloidal iron. Genomewide analysis demonstrated significant evidence of linkage to chromosome region 12q21.33 and evidence suggestive of linkage to chromosome region 8q22.3. Fine mapping of the chromosome 12 locus confirmed significant linkage; the largest multipoint log odds ratio score was 5.6 at D12S351. The linkage support interval was approximately 3.5 Mb (3.5 cM) in length between flanking markers D12S1812 and D12S95, roughly the entire chromosome band 12q21.33. No coding region mutations were identified in four candidate genes—*KERA*, *LUM*, *DCN*, *EPYC*—located in the chromosome 12 linkage support interval.

Conclusions. Linkage and haplotype analyses identified 12q21.33 as a locus for PACD. However, no mutations were identified in the candidate genes (*KERA*, *LUM*, *DCN*, *EPYC*) within this region. (*Invest Ophthalmol Vis Sci.* 2010;51: 4006–4012) DOI:10.1167/iovs.09-4067

Posterior amorphous corneal dystrophy (PACD) is a rare autosomal dominant corneal dystrophy and has been reported in only 11 families to date.[1–9] Characteristic clinical features include partial or complete posterior lamellar corneal opacification, decreased corneal thickness (typically <500 μm centrally), and average corneal curvature <41 D.[3,4,8,9] Other reported manifestations include iris abnormalities, such as iridocorneal adhesions, correctopia, and iris atrophy.[8,9] Even though subtle endothelial changes have been reported in some patients,[7–9] corneal endothelial function is not typically affected,[4,7,8] and most affected patients retain good corrected vision throughout their lives. Light and electron microscopic examinations of the corneas in affected patients have revealed an irregular arrangement of the collagen fibrils in the posterior corneal stromal lamellae and the presence of an abnormal collagenous layer either within Descemet's membrane or between it and the corneal endothelium.[6,7] Because no intracellular or extracellular deposits have been detected with the use of hematoxylin-eosin, Masson trichrome, or Alcian blue stains, posterior stromal opacification has been attributed to the disorganization of the posterior stromal lamellae, similar to the cause of the stromal opacification in congenital hereditary stromal dystrophy.

Many of the clinical features associated with PACD are also associated with cornea plana, such as corneal flattening (with associated high hyperopia), iridocorneal adhesions, and iris atrophy. Although the genetic basis of the autosomal dominant form of cornea plana (CNA1 [Mendelian Inheritance in Man (MIM) 121499]) remains unknown, the autosomal recessive form (CNA2 [MIM 217300]) has been associated with mutations in the keratocan gene (*KERA* [MIM 603288]).[10–15]

We sought to identify the genetic basis of PACD through genomewide linkage analysis and screening of positional and functional candidate genes *KERA*, lumican (*LUM* [MIM 600616]), decorin (*DCN* [MIM 125255]), and epiphycan (*EPYC* [also known as *DSPG3*; MIM 601657]) in affected and unaffected members of a large, previously unreported family with PACD. We further characterized the clinical and histopathologic features of PACD through description of the anterior segment clinical findings in affected members of this five-generation pedigree and by light and electron microscopic examinations of an excised corneal specimen.

Materials and Methods

The researchers followed the tenets of the Declaration of Helsinki in the treatment of the subjects reported herein. Study approval was obtained from the Institutional Review Board at the University of California at Los Angeles (UCLA IRB 94-07-243-23 and 94-07-243-24).

Patient Identification and DNA Collection

After informed consent was obtained, a slit lamp examination was performed for each study participant to determine the affected status.

From the [1]Jules Stein Eye Institute and the [3]Department of Human Genetics, David Geffen School of Medicine, University of California at Los Angeles, Los Angeles, California; the [2]Central Pennsylvania Eye Institute, Hershey, Pennsylvania; and the [4]Department of Ophthalmology, Milton S. Hershey Medical Center, Hershey, Pennsylvania.

Supported by National Institutes of Health Grant K08 EY016079 (AJA).

Submitted for publication June 4, 2009; revised August 5 and October 3, 2009, and February 11, 2010; accepted March 10, 2010.

Disclosure: **A.J. Aldave,** None; **G.O.D. Rosenwasser,** None; **V.S. Yellore,** None; **J.C. Papp,** None; **E.M. Sobel,** None; **M.N. Pham,** None; **M.C. Chen,** None; **S. Dandekar,** None; **R. Sripracha,** None; **S.A. Rayner,** None; **J.W. Sassani,** None; **M.B. Gorin,** None

Corresponding author: Anthony J. Aldave, Jules Stein Eye Institute, 100 Stein Plaza, UCLA, Los Angeles, CA 90095; aldave@jsei.ucla.edu.

The diagnosis of PACD was based on the presence of one or more of the following clinical features in each eye: scleralization of the peripheral cornea; partial or complete posterior corneal lamellar haze; decreased central corneal thickness (≤500 μm); significant corneal flattening (average corneal curvature <38 D); or an iris abnormality, such as iris atrophy, coloboma, or correctopia. Blood was obtained from 37 subjects. For an additional 17 subjects for whom phlebotomy could not be performed or was refused, DNA was collected using buccal epithelial swabs (CytoSoft Cytology Brush; Medical Packaging Corporation, Camarillo, CA) and saliva collection kits (Oragene; DNA Genotek Inc., Kanata, ON, Canada). DNA was prepared from peripheral blood leukocytes and buccal epithelial cells using DNA kits (PaxGene [Qiagen, Valencia, CA] and DNA Blood Mini Kits [Qiagen], respectively).

Genomewide Linkage Analysis, PCR Amplification, and Genotyping

Genomewide linkage analysis was performed using a linkage mapping set (MD-10; Applied Biosystems, Foster City, CA) consisting of 400 microsatellite markers that span the entire human genome at a 10 cM average marker density. Polymerase chain reaction (PCR) amplification of each marker was performed using a forward primer of each pair that was labeled with the fluorescent dye tag 6-FAM, VIC, or NED. Reactions were carried out using 15 ng preamplified genomic DNA (amplified using a DNA amplification kit [GenomiPhi; GE Healthcare Bio-Sciences, Piscataway, NJ]).

Genotyping was performed at the UCLA Sequencing and Genotyping Core facility. PCR fragments were analyzed on capillary DNA analyzers (ABI-3700 and 3ABI-730; Applied Biosystems). Each run included two positive control samples (individual 2 in CEPH family 1347; Coriell Institute, Camden, NJ). Genotype calling was performed using Applied Biosystems software (Genotyper and GeneMapper). All genotypes were verified by human inspection in two independent readings.

Fine-Mapping Linkage Analysis, PCR Amplification, and Genotyping

Thirty microsatellite markers spanning an 18-cM region of chromosome 8 surrounding marker D8S1784 and 40 microsatellite markers spanning an 18-cM region of chromosome 12 surrounding marker D12S351 were selected from the National Center for Biotechnology Information (NCBI) public database. Locations of the markers were determined by referencing physical (NCBI Map Viewer; NCBI build 37.1) and genetic (Marshfield Clinic Center for Human Genetics) maps.

PCR amplification of all markers was performed using primer sequences obtained from the uniSTS section of the NCBI database. The forward primer of each pair was labeled with one of the fluorescent dye tags—6-FAM, VIC, or NED—from Applied Biosystems. Each reaction was carried out in a 25-μL mixture containing 60 to 70 ng preamplified genomic DNA (amplified with GenomiPhi DNA amplification kit from Amersham Biosciences Corp., Piscataway, NJ), 0.25 μL each primer (10 pM/μL), 0.5 U *Taq* DNA polymerase, and 2.5 μL 10× PCR buffer (Sigma-Aldrich Co., St. Louis, MO). Thermal cycling was performed (iCycler; Bio-Rad, Hercules, CA) under the following conditions: initial denaturation for 5 minutes at 95°C, 30 cycles at 94°C for 30 seconds, 58°C for 30 seconds, 72°C for 30 seconds, and a final extension for 5 minutes at 72°C.

Genotyping was performed at the UCLA Sequencing and Genotyping Core. PCR fragments were analyzed on capillary DNA analyzers (ABI 3700 and 3730; Applied Biosystems). Each run included two positive control samples (individual 2 in CEPH family 1347; Coriell Institute). Genotype calling was performed using Applied Biosystems (Genotyper and GeneMapper) software. All genotyping was performed blind to family structure and was verified by human inspection in two independent readings.

Statistical Analysis

Before the performance of linkage analysis, possible genotyping inconsistencies were evaluated using SimWalk 2.91.[16] All genotypes with a posterior probability of mistyping greater than 0.5 were reevaluated by review of the raw genotype data. If the possible mistyping was not resolved by review, the suspect genotypes were set to unknown. On reevaluation of the raw data, 21 genotypes were changed, and 118 genotypes were set to unknown, representing a mistyping rate of 0.55%.

Single-point linkage analysis was performed using Mendel 10,[17] and multipoint linkage analysis was performed using SimWalk 2.91. For both single-point and multipoint analyses, an autosomal partial-dominance model was used with a disease allele frequency of 0.001, a phenocopy rate of 0.001, and penetrance rates of 0.8 for heterozygotes and 0.999 for homozygotes. Haplotype analysis was performed using SimWalk 2.91.

Candidate Gene Screening

PCR Amplification. Using DNA from affected and unaffected individuals (II-10, III-4, III-13, III-15, IV-3, and IV-9 in Fig. 1), the coding regions of the *KERA*, *LUM*, *DCN*, and *EPYC* genes were amplified by PCR using custom-designed primers (sequences available on request). All primers were designed so that they would bind to intronic segments 60 to 80 nucleotides on either side of the intron-exon boundary to ensure complete reading of the exons. Each reaction was carried out in a 25-μL mixture containing 50 mM Tris-HCl (pH 9.0, 25°C), 20 mM NH_4Cl, 2.5 mM $MgSO_4$, 200 μM each dNTP, 0.5 M betaine, 2.5 μL DMSO, 150 mM trehalose, 0.002% Tween-20, 0.12 μM each primer, 0.5 U genomic DNA polymerase (REDTaq; Sigma-Aldrich), and approximately 60 ng genomic DNA. Thermal cycling was then performed (iCycler Thermal Cycler; Bio-Rad).

DNA Sequencing. PCR products were purified by incubating 15 to 30 ng DNA with 5 U exonuclease I and 0.5 U shrimp alkaline phosphatase (USB Corp., Cleveland, OH) for 15 minutes at 37°C. After inactivation of the nucleases (80°C for 15 minutes), sequencing reactions were performed by the addition of 1 μL reaction mix (BigDye

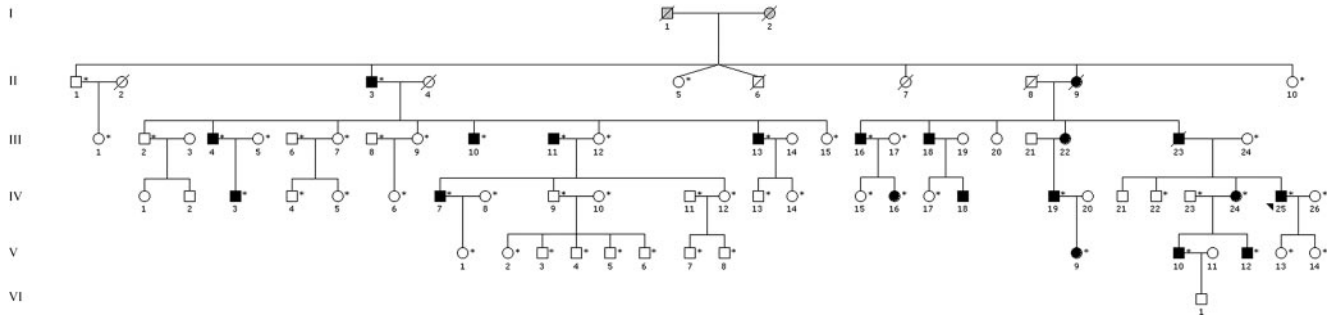

FIGURE 1. Pedigree of family with PACD. *Black symbols*: affected individuals; *gray symbols*: individuals of unknown affected status; *open symbols*: unaffected individuals. *Arrowhead*: proband. *Asterisks*: individuals who underwent slit lamp examination, DNA collection, and genotyping.

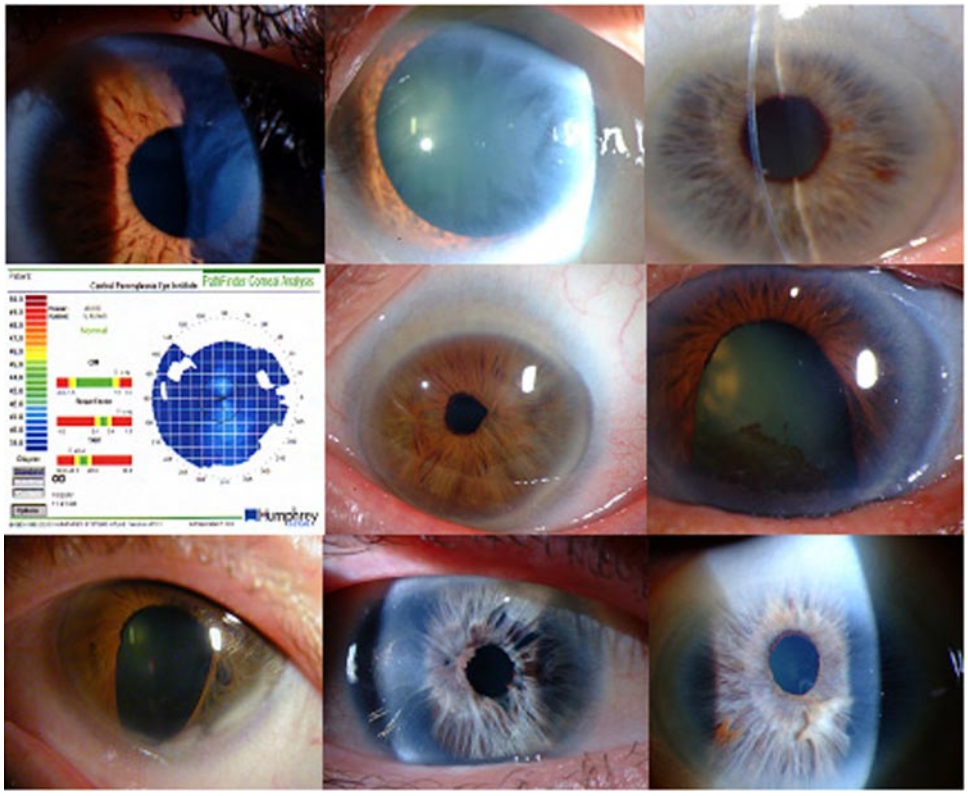

FIGURE 2. Slit lamp photomicrograph of individuals IV-3 (*top row*, *left*) and III-10 (*top row*, *middle*) shows partial posterior corneal lamellar opacification. The posterior lamellar corneal stromal opacification is highlighted by a thin slit beam in individual III-23 (*top row*, *right*). Corneal topographic image of individual III-4 (*middle row*, *left*) shows significant corneal flattening in the right eye, with an average keratometry value of 40.4 D. Slit lamp photomicrograph of individual III-13 (*middle row*, *center*) shows superior corneal scleralization, characterized by peripheral corneal opacification and vascularization. Inferior iris colobomas are pictured for individuals II-3 (*middle row*, *right*) and III-13 (*bottom row*, *left*). Diffuse iris stromal atrophy, disruption of the normal iris architecture, and correctopia are observed in individuals IV-25 (*bottom row*, *center*) and III-23 (*bottom row*, *right*).

Terminator Mix v3.1; Applied Biosystems), 1 μL dilution buffer (SeqSaver; Sigma-Aldrich), and 0.2 μL primer solution (10 pM/μL). Samples were denatured at 96°C for 2 minutes, then cycled 25 times at 96°C for 10 seconds, 50°C for 5 seconds, and 60°C for 4 minutes. Unincorporated nucleotides were removed using a reagent and a solid-phase reversible immobilization (SPRI) plate (CleanSeq; Agencourt Bioscience Corporation, Beverly, MA) according to the manufacturer's instructions. Amplified DNA was then resuspended in 0.1 mM EDTA and analyzed on a genetic analyzer (ABI-3100; Applied Biosystems). Nucleotide sequences were read manually and with a software program (Mutation Surveyor v2.2; Softgenetics, State College, PA). The sequences were compared with the published cDNA sequence for *KERA* (NM_007035), *LUM* (NM_002345), *DCN* (NM_001920), and *EPYC* (NM_004950).

Light and Electron Microscopic Analysis

A corneal button, removed from one of the affected individuals (Fig. 1, III-13) at the time of penetrating keratoplasty, was bisected. Half the button was fixed in 10% neutral-buffered formaldehyde and analyzed with light microscopy after staining with hematoxylin and eosin, Congo red, periodic acid-Schiff, Alcian blue, and colloidal iron stains. The other half was fixed in 2.5% glutaraldehyde and processed for transmission electron microscopy.

RESULTS

Clinical Characteristics

Twenty individuals in four consecutive generations were identified as affected, and 54 informative individuals were ascertained within the family (Fig. 1). Each affected individual demonstrated posterior corneal stromal lamellar opacification that appeared either at or just anterior to Descemet's membrane (Fig. 2). Opacification was incomplete in every affected individual, with areas of corneal lucency interspersed between the regions of swirling posterior lamellar corneal opacification. In

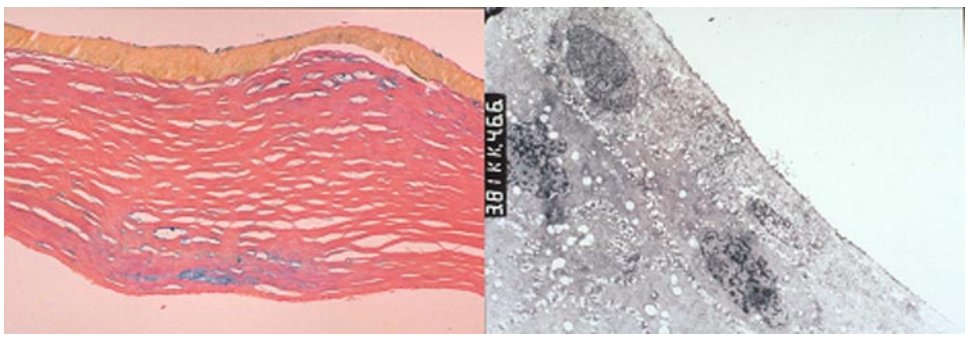

FIGURE 3. *Left*: histophotomicrograph of corneal button from individual III-13, demonstrating staining of the anterior and posterior stromal regions with the colloidal iron stain (original magnification, ×40). *Right*: electron micrograph of corneal button from individual III-13, demonstrating cystic structures in the corneal endothelial cells, which likely represent dilated mitochondria (original magnification, ×3810).

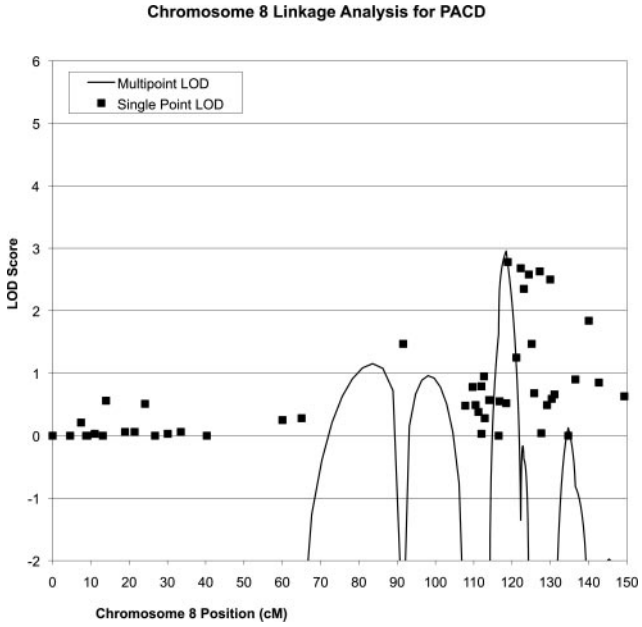

FIGURE 4. Linkage analysis results for PACD candidate region on chromosome 8; single-point performed using Mendel 10 (*filled squares*), multipoint performed using SimWalk 2.91 (*solid line*). The 50 markers used for the linkage analysis on chromosome 8 are shown. Chromosomal positions are listed as distance in Haldane cM from first marker.

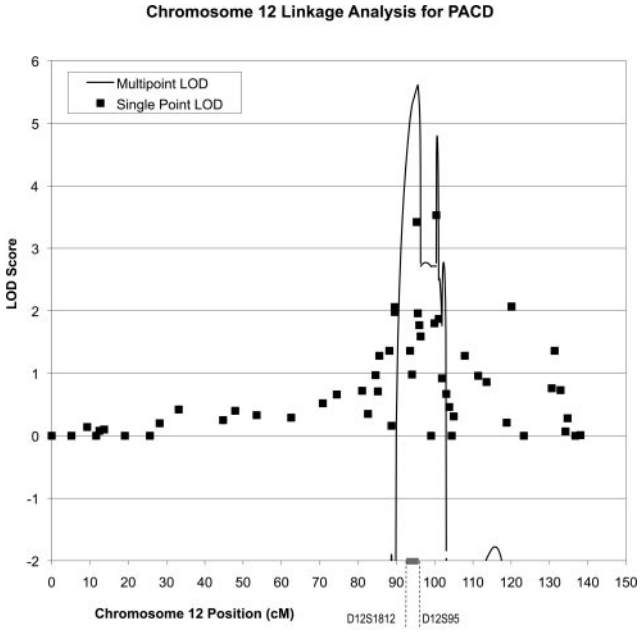

FIGURE 5. Linkage analysis results for PACD candidate region on chromosome 12; single-point performed using Mendel 10 (*filled squares*), and multipoint performed using SimWalk 2.91 (*solid line*). The 52 markers used for the linkage analysis on chromosome 12 are shown. The 3.5-Mb *gray bar* on the *x*-axis indicates the linkage support interval, defined as the region in which the multipoint LOD score is within 1 unit of the peak value. Chromosomal positions are listed as distance in Haldane cM from first marker.

each affected individual, the opacification was bilateral and symmetric, and appeared similar between both younger (Fig. 1, generation V) and older (Fig. 1, generation II) members of the family. Affected individuals also demonstrated diffuse corneal thinning, with an average central corneal thickness of 453 μm (range, 364–543 μm) compared with the average central corneal thickness of 563 μm (range, 509–602 μm) in unaffected individuals. Corneal topographic imaging in select affected individuals showed significant corneal flattening in each eye, with an average corneal curvature of 39.12 D (range, 35.87–43.56 D) (Fig. 2). Most affected individuals demonstrated bilateral superior corneal scleralization (Fig. 2), and several demonstrated iris abnormalities, including correctopia and iris coloboma (Fig. 2). Two of the affected individuals required corneal transplantation for visually significant corneal opacification (Fig. 1, III-13 and IV-3).

Fifteen of the affected individuals provided DNA for genetic analysis. Thirty-nine individuals who were examined and found to be unaffected also provided DNA for genetic analysis (Fig. 1).

Light and Electron Microscopy

Individual III-13 (Fig. 1) underwent corneal transplantation at age 60 for visually significant corneal opacification. Light microscopic examination of the excised corneal specimen revealed irregularity of the posterior stromal lamellae. Although Descemet's membrane appeared mildly irregular, an abnormal collagenous layer was not identified either within or beneath it. Colloidal iron staining of the anterior and posterior corneal stromal regions was seen, although no staining was noted with Alcian blue, periodic acid-Schiff, or Congo red (Fig. 3).

Electron microscopic examination revealed the presence of amorphous extracellular material between the stromal lamellae in the anterior cornea. Cystic membrane-bound structures were noted in the corneal endothelial cells, suggestive of dilated mitochondria (Fig. 3).

Genomewide Linkage Analysis

Linkage analysis on the genomewide marker set yielded a large single-point log odds ratio (LOD) score of 3.42 (with $\theta = 0$) at

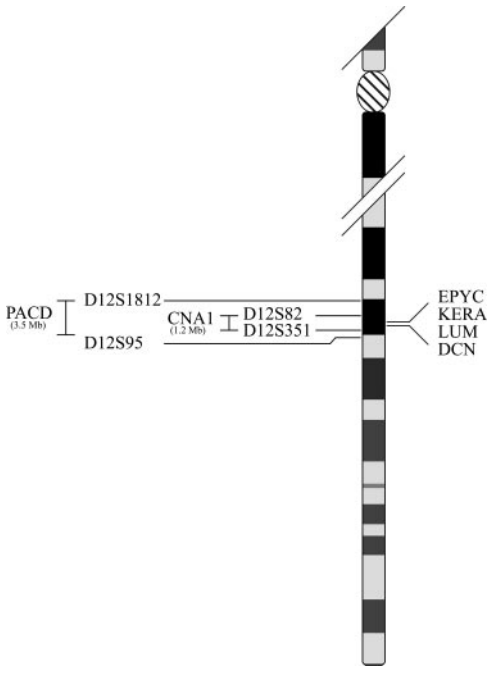

FIGURE 6. This ideogram of chromosome 12 shows the positions of four candidate genes (*KERA*, *LUM*, *DCN*, and *EPYC*), the CNA1 support interval (flanked by markers D12S82 and D12S351), and the newly reported PACD linkage support interval (flanked by markers D12S1812 and D12S95).

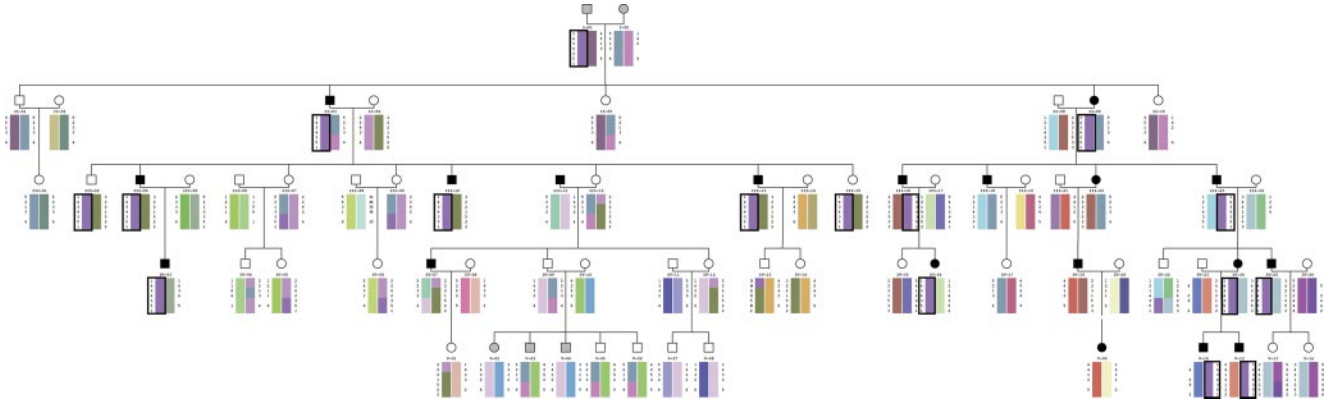

FIGURE 7. Haplotype drawing demonstrating the most likely configuration of this pedigree on a 10-cM interval on chromosome 8. This interval contains the seven loci. *Top to bottom*: D8S1844, D8S1784, D8S200, D8S85, D8S1122, D8S2320, and D8S1467. The boxed consensus haplotype is seen in its entirety in 13 of the 19 affected individuals (*black symbols*), in two unaffected individuals (*white symbols*), and in one founder individual of unknown affection status (*gray symbol*). This chromosomal interval includes the loci with the highest single-point and multipoint LOD scores on chromosome 8. The shared haplotype did not extend beyond this interval. Note that 10 individuals from Figure 1, for whom no DNA was collected and whose haplotype could not be inferred from the rest of the pedigree, are not included in this figure.

marker D12S351 on chromosome 12q21.33. The next largest single-point LOD score was 2.68 (with $\theta = 0$) at marker D8S1784 on chromosome 8q22.3. No other single-point LOD score was above 2.5. The largest multipoint LOD score using the genomewide marker set was 3.82 at D12S351, the same marker that provided the highest single-point LOD score. Multipoint scores in this region identified an 11-cM support interval between flanking markers D12S1708 and D12S346. No positive LOD scores were identified on chromosome 8 with multipoint linkage analysis when using the genomewide marker set.

Fine Mapping in Chromosome 8q22.3 and 12q21.33 Regions

Fine mapping in the region of chromosome 8q22.3 generated a maximum single-point LOD score of 2.78 (with $\theta = 0$) at D8S1814. D8S1814 is only 370 kb from D8S1784, the location of the peak single-point LOD in this region in the genomewide scan. After including the fine mapping markers, the largest multipoint LOD score was 2.95 at D8S200, which is 2.1 Mb from D8S1814. Figure 4 graphs these results.

Fine mapping in the region of chromosome 12q21.33 generated a maximum single-point LOD score of 3.53 (with $\theta = 0$) at D12S1716, which is 5.1 Mb from D12S351, the location of the peak single-point LOD in this region in the genomewide scan. After including the fine mapping markers, the largest multipoint LOD score is 5.62 at D12S322. D12S322 is only 300 kb from D12S351. The multipoint scores in this region identify a 3.5-Mb (3.5 cM) linkage support interval between flanking markers D12S1812 and D12S95, roughly the entire chromosome band 12q21.33. Figure 5 graphs these results. The four functional candidate genes—*KERA*, *LUM*, *DCN*, and *EPYC*—are within this 3.5-Mb linkage support interval on chromosome 12 (Fig. 6).

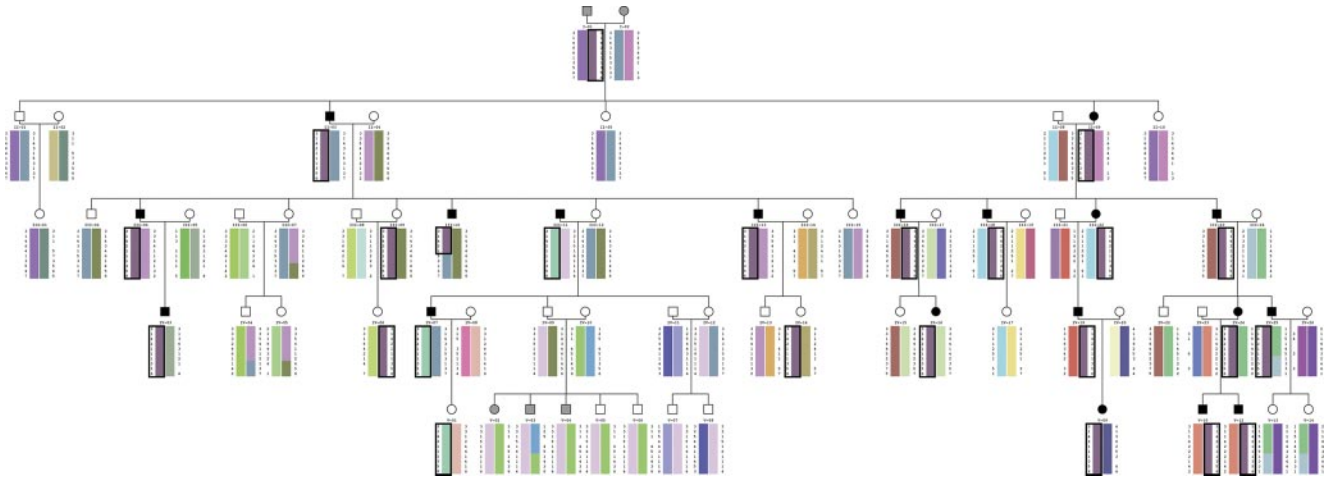

FIGURE 8. Haplotype drawing demonstrating the most likely configuration of this pedigree on a 10-cM interval on chromosome 12. This interval contains the 10 loci. *Top to bottom*: D12S1678, D12S316, D12S351, D12S322, D12S2077, D12S95, D12S101, D12S309, D12S1716, and D12S1051. The boxed consensus haplotype is seen in its entirety in 18 of the 19 affected individuals (*black symbols*), in four unaffected individuals (*white symbols*), and in one founder individual of unknown affection status (*gray symbol*). This chromosomal interval includes the loci with the highest single-point and multipoint LOD scores on chromosome 12. The shared haplotype did not extend beyond this interval. The appearance of the disease-carrying haplotype in the married-in III-11 strongly implies an unknown genetic relationship between III-11 and the other affected individuals. Note that 10 individuals depicted in Figure 1, for whom no DNA was collected and whose haplotype could not be inferred from the rest of the pedigree, are not included in this figure.

Haplotype Analysis in Chromosome 8q22.3 and 12q21.33 Regions

Haplotype analysis of the chromosome 8q22.3 region found no consistent haplotype among the affected individuals. Given our genotyping results, Figure 7 shows the most likely haplotype configuration in the 10-cM interval from D8S1844 to D8S588. This interval includes the loci with the highest single-point and multipoint LOD scores on chromosome 8. Thirteen of the 19 analyzed affected individuals share a haplotype at all seven genotyped loci in this region. The shared haplotype did not extend beyond this interval. The other six affected individuals did not exhibit any consistent haplotypes in this region. Among all unaffected individuals, the entire consensus haplotype is seen only twice, in individuals III-02 and III-15 in Figure 7.

Haplotype analysis of the chromosome 12q21.33 region showed a clear conserved haplotype segregating through the pedigree in almost all affected individuals. Given our genotyping results, Figure 8 shows the most likely haplotype configuration in the 10-cM interval from D12S1678 to D12S1051. This interval includes the loci with the highest single-point and multipoint LOD scores on chromosome 12. Eighteen of the 19 analyzed affected individuals share a haplotype at all 10 genotyped loci in this region. The shared haplotype did not extend beyond this interval. The remaining affected individual, III-10, does not share the lower half of this conserved haplotype. As seen in Figure 8, the most likely configuration is individual III-10 does share the top half of the conserved haplotype. However, because of the extent of homozygosity in this region and some missing genotypes, it is also possible that III-10 did not inherit any part of this chromosomal region from the conserved haplotype in his father.

The conserved haplotype is found only once in each affected individual, supporting a dominant inheritance model for this trait. For all but two of the affected individuals, this haplotype originated in one of the pedigree founders, either I-1 or I-2. (Given that both founders have unknown affection status and were not genotyped, based on the current evidence they are equally likely to have introduced the haplotype into the pedigree.) The conserved haplotype was also observed in an affected married-in individual, III-11, and was then passed on to his affected son IV-7. (This suggests individual III-11 is genetically related to the other affected individuals, but that relationship is unknown.) The conserved haplotype was found in four unaffected individuals—III-09, IV-06, IV-14, and V-01—in Figure 8, supporting a reduced penetrance inheritance model for this trait. All four unaffected individuals with the conserved haplotype are female.

KERA, *LUM*, *DCN*, and *EPYC* Screening

Three previously described single nucleotide substitutions were identified in the coding and untranslated regions of both *KERA* and *LUM*, two novel sequence variants were identified in the 5′ untranslated region of *KERA*, and a novel synonymous substitution was identified in *DCN*. However, none of these sequence variants was considered pathogenic because none was found to segregate with the affected phenotype (Table 1). No sequence variants were identified in *EPYC*.

Discussion

Since the initial discovery of the genetic basis of the *TGBFI* corneal dystrophies in 1997, vision science researchers have identified the genetic basis of approximately three-quarters of the corneal dystrophies.[18] PACD is one of the very few corneal dystrophies for which no genetic investigations have been published, most likely because of the rarity of the disorder; only 38 affected individuals from 11 families with PACD are reported in the literature.[1–9] We performed a microsatellite-based genomewide linkage analysis on a large family with 20 PACD affected individuals and identified two potential genetic loci for PACD. The genomewide analysis found significant evidence for linkage to chromosome 12q21.33 (LOD score >3.3) and suggestive evidence for linkage to chromosome 8q22.3 (LOD score 2.2–3.3). Fine mapping the chromosome 8q22.3 region did not result in evidence for significant linkage with either single-point or multipoint analysis. Haplotype analysis of chromosome 8 did not yield a consistent haplotype across the affected individuals. However, fine mapping the chromosome 12q21.33 region resulted in an increase in the maximum multipoint LOD score to 5.62, well above the standard threshold for genomewide significant evidence for linkage. These results provide a 3.5-Mb linkage support interval for a locus influencing PACD between flanking markers D12S1812 and D12S95, roughly the entire chromosome band 12q21.33. Haplotype analysis of chromosome 12 showed a highly conserved ancestral haplotype shared among the affected individuals, consistent with the linkage support interval.

KERA, the keratocan gene, is 1 of 11 genes that have been mapped to the 3.5-Mb linkage support interval in 12q21.33 (Human Genome Browser; NCBI build 37.1). Mutations in *KERA* have been shown to cause CNA2, the autosomal recessive form of cornea plana.[10–15] Given the presence of many clinical features that are common to both cornea plana and PACD, *KERA* was selected as a candidate gene for PACD even before results of the genomewide linkage analysis were obtained. The demonstration of significant evidence of linkage of a PACD locus to the region of chromosome 12 to which *KERA* had previously been mapped further implicates a possible role

Table 1. Summary of Sequence Variants Identified in *KERA, LUM, DCN,* and *EPYC*

Gene	Nucleotide Change	Amino Acid Change	refSNP ID	Individuals Screened	
				Affected (n = 3)	Unaffected (n = 3)
DCN	c.33A>G	p.Ala11Ala	None	0	1 (heterozygous)
EPYC	None	—	—	—	—
KERA	c.−430T>C	—	None	0	2 (both heterozygous)
	c.−429A>C	—	rs1990548	0	2 (both heterozygous)
	c.−78delT	—	None	3 (all heterozygous)	3 (all heterozygous)
	c.69G>A	p.Val23Val	rs2735333	0	3 (2 heterozygous)
	c.75G>A	p.Gln25Gln	rs12320366	0	2 (both heterozygous)
LUM	c.−152 −153dupCC	—	rs3832846	3 (all homozygous)	3 (all homozygous)
	c.625G>A	—	rs11478	1 (homozygous)	0
	c.649T>C	—	rs3168534	1 (homozygous)	0

for *KERA* (or a nearby functionally related gene) in the pathogenesis of PACD. Located adjacent to *KERA* on chromosome 12 are genes *LUM*, *DCN*, and *EPYC*, encoding three other members of the small leucine-rich proteoglycan (SLRP) family, lumican, decorin, and epiphycan, respectively. Proteoglycans, which modulate collagen fibril development and are involved in the maintenance of corneal clarity, consist of core proteins, such as keratocan, lumican, and decorin, bound to glycosaminoglycans, which form the ground substance of the cornea.[19] Interference with the function of the genes encoding the SLRPs leads to corneal opacification, as has been demonstrated in *LUM*-deficient mice[20] and in patients with congenital hereditary stromal dystrophy, which has been shown to be secondary to mutations in *DCN*.[21,22] Thus, because the products of these genes have been shown to regulate corneal transparency and are all located within the linkage support interval, the coding region of each was screened in the same affected and unaffected individuals who had been screened for coding region mutations in *KERA*.

Although no coding region mutations were identified in *KERA*, *LUM*, *DCN*, and *EPYC*, it is still possible that one of these genes is involved in the pathogenesis of PACD. Only six genes have been mapped to the 1.2-Mb candidate interval for CNA1: *KERA*, *LUM*, *DCN*, *EPYC*, and two predicted genes, chromosome 12 open-reading frame 37 (*C12orf37*) and chromosome 12 open-reading frame 12 (*C12orf12*) (NCBI Map Viewer; NCBI build 37.1).[23] Therefore, it seems surprising that coding region mutations have not been identified in *KERA*, *LUM*, *DCN*, or *EPYC* in families with CNA1.[10,15] However, given the significant phenotypic similarities between CNA1 and PACD and the location of *KERA*, *LUM*, *DCN*, and *EPYC* within the linkage support interval for each, these genes remain attractive positional and functional candidate genes for both conditions. Large-scale resequencing of the chromosomal region containing *KERA*, *LUM*, *DCN*, and *EPYC* is planned to exclude the possibility of a pathogenic copy number variant or a noncoding mutation that affects the function of the encoded protein product of one of the four genes through, for example, alteration of expression and exon skipping. We also encourage investigators who have reported families with posterior amorphous corneal dystrophy to perform fine mapping of the chromosome 12q21.33 candidate locus region using the same markers we did to demonstrate the replication of linkage to this locus and to further narrow the candidate interval through haplotype analysis.

Acknowledgments

The authors thank Lara Rosenwasser for her assistance in collecting clinical data.

References

1. Erdem U, Muftuoglu O, Hurmeric V. In vivo confocal microscopy findings in a patient with posterior amorphous corneal dystrophy. *Clin Exp Ophthalmol.* 2007;35:99–102.
2. Oliveira LA, Vieira LA, Freitas D, Sousa LB. [Posterior amorphous corneal dystrophy: case report]. *Arq Bras Oftalmol.* 2006;69:945–947.
3. Castelo Branco B, Chalita MR, Casanova FH, Castelo Branco AB, Allemann N, de Freitas D. Posterior amorphous corneal dystrophy: ultrasound biomicroscopy findings in two cases. *Cornea.* 2002;21:220–222.
4. Moshegov CN, Hoe WK, Wiffen SJ, Daya SM. Posterior amorphous corneal dystrophy: a new pedigree with phenotypic variation. *Ophthalmology.* 1996;103:474–478.
5. Grimm BB, Waring GO 3rd, Grimm SB. Posterior amorphous corneal dysgenesis. *Am J Ophthalmol.* 1995;120:448–455.
6. Roth SI, Mittelman D, Stock EL. Posterior amorphous corneal dystrophy: an ultrastructural study of a variant with histopathological features of an endothelial dystrophy. *Cornea.* 1992;11:165–172.
7. Johnson AT, Folberg R, Vrabec MP, Florakis GJ, Stone EM, Krachmer JH. The pathology of posterior amorphous corneal dystrophy. *Ophthalmology.* 1990;97:104–109.
8. Dunn SP, Krachmer JH, Ching SS. New findings in posterior amorphous corneal dystrophy. *Arch Ophthalmol.* 1984;102:236–239.
9. Carpel EF, Sigelman RJ, Doughman DJ. Posterior amorphous corneal dystrophy. *Am J Ophthalmol.* 1977;83:629–632.
10. Aldave AJ, Sonmez B, Bourla N, et al. Autosomal dominant cornea plana is not associated with pathogenic mutations in DCN, DSPG3, FOXC1, KERA, LUM, or PITX2. *Ophthalmic Genet.* 2007;28:57–67.
11. Khan A, Al-Saif A, Kambouris M. A novel KERA mutation associated with autosomal recessive cornea plana. *Ophthalmic Genet.* 2004;25:147–152.
12. Khan AO, Aldahmesh M, Al-Saif A, Meyer B. Pellucid marginal degeneration coexistent with cornea plana in one member of a family exhibiting a novel KERA mutation. *Br J Ophthalmol.* 2005;89:1538–1540.
13. Khan AO, Aldahmesh M, Meyer B. Recessive cornea plana in the Kingdom of Saudi Arabia. *Ophthalmology.* 2006;113:1773–1778.
14. Lehmann OJ, El-ashry MF, Ebenezer ND, et al. A novel keratocan mutation causing autosomal recessive cornea plana. *Invest Ophthalmol Vis Sci.* 2001;42:3118–3122.
15. Pellegata NS, Dieguez-Lucena JL, Joensuu T, et al. Mutations in KERA, encoding keratocan, cause cornea plana. *Nat Genet.* 2000;25:91–95.
16. Sobel E, Lange K. Descent graphs in pedigree analysis: applications to haplotyping, location scores, and marker-sharing statistics. *Am J Hum Genet.* 1996;58:1323–1337.
17. Lange K, Cantor R, Horvath S, et al. Mendel version 4.0: a complete package for the exact genetic analysis of discrete traits in pedigree and population data sets. *Amer J Hum Genetics*. 2001;69(suppl):504.
18. Aldave AJ, Sonmez B. Elucidating the molecular genetic basis of the corneal dystrophies: are we there yet? *Arch Ophthalmol.* 2007;125:177–186.
19. Iozzo RV. Matrix proteoglycans: from molecular design to cellular function. *Annu Rev Biochem.* 1998;67:609–652.
20. Chakravarti S, Zhang G, Chervoneva I, Roberts L, Birk DE. Collagen fibril assembly during postnatal development and dysfunctional regulation in the lumican-deficient murine cornea. *Dev Dyn.* 2006;235:2493–2506.
21. Bredrup C, Knappskog PM, Majewski J, Rodahl E, Boman H. Congenital stromal dystrophy of the cornea caused by a mutation in the decorin gene. *Invest Ophthalmol Vis Sci.* 2005;46:420–426.
22. Rodahl E, Van Ginderdeuren R, Knappskog PM, Bredrup C, Boman H. A second decorin frame shift mutation in a family with congenital stromal corneal dystrophy. *Am J Ophthalmol.* 2006;142:520–521.
23. Tahvanainen E, Villanueva AS, Forsius H, Salo P, de la Chapelle A. Dominantly and recessively inherited cornea plana congenita map to the same small region of chromosome 12. *Genome Res.* 1996;6:249–254.